

# Magic Mirror on the Wall, How to Benchmark Quantum Error Correction Codes, Overall ?

Avimita Chatterjee and Swaroop Ghosh

School of EECS, The Pennsylvania State University, USA

**Quantum Error Correction Codes (QECCs) are fundamental to the advancement of quantum computing, safeguarding quantum states from the detrimental impact of noise and errors. The right choice of QECC, tailored to specific scenarios influenced by noise levels and qubit constraints, is as vital as the technological advancements themselves. This paper introduces a novel and comprehensive methodology for benchmarking QECCs, featuring a set of universal parameters. Utilizing eight distinguished QECCs, we propose a suite of eight parameters for a thorough analysis. Our work not only establishes a universal benchmarking methodology but also underscores the nuanced balance inherent in quantum error correction. The paper highlights that there is no one-size-fits-all solution; the selection of a QECC is contingent upon the specific constraints and circumstances of each case.**

Keywords: Quantum error correction codes (QECCs), Benchmarking, Parameters.

## 1 Introduction

Quantum computing harnesses the principles of quantum mechanics to execute tasks that are beyond the capabilities of classical computing. This advanced technology finds applications in various fields, including molecule simulation for drug development, financial optimization enhancements, machine learning acceleration, improvement of optimization tasks, and revolutionary changes in supply chain management, among others [58, 54, 62, 30, 4]. However, commercialization of these quantum computing developments incurs

Avimita Chatterjee: [amc8313@psu.edu](mailto:amc8313@psu.edu)

Swaroop Ghosh: [szg212@psu.edu](mailto:szg212@psu.edu)

challenges such as qubit stability and quantum noise [19, 47]. Quantum Error Correction Codes (QECCs) are crucial for achieving fault-tolerant quantum computing in the face of unavoidable qubit noise [45, 23]. Traditional error correction methods [33] encounter unique challenges in the quantum realm, primarily due to constraints like the no-cloning theorem [79] and the wavefunction collapse that occurs during qubit measurement [76]. Research in this field has led to the creation of various quantum codes, such as the five-qubit code, Bacon-Shor code, topological code, surface code, color code, and heavy-hexagon code. These codes have shown effectiveness in correcting single errors [69, 2, 6, 40, 42, 11].

### 1.1 Motivation

Many quantum error-correcting codes have been proposed, each offering unique advantages and trade-offs. These range from the well-known Shor and Steane codes to more recent innovations like topological codes. However, this diversity leads to a critical question: “Which code is most suitable for a given quantum computing scenario?” This question underscores the need for a comprehensive, standardized benchmarking methodology. While numerous studies have individually assessed various QECCs, there is a lack of a unified methodology that allows for an objective, comparative analysis across codes. Such a comparison is vital not just for current quantum computing research but also for guiding future developments in QECCs.

### 1.2 Contribution

This paper introduces a comprehensive benchmarking methodology designed for all QECCs. Our methodology includes key parameters such as error correction capability, resource efficiency,

error threshold, and scalability, ensuring a well-rounded evaluation of each code's performance and practical feasibility. Through this methodology, we extensively compare various notable QECCs and their variations, offering insights into their behavior under different scenarios and highlighting their strengths and weaknesses. This methodology serves as a standard for assessing all QECCs and their variations, encompassing both existing and future ones.

To our knowledge, this is the first instance of a unified benchmarking methodology for all quantum error correction codes. With the ongoing evolution of quantum computing, new codes and their variations will continually arise. Our methodology offers a systematic approach to evaluate these codes, aiming to ensure that advancements in quantum computing are substantial and effectively address the quantum error challenge. In this study, we analyze eight prominent QECCs using eight distinct parameters, providing a clear comparative analysis. This study assists in choosing the most suitable QECC for their specific quantum computing applications.

### 1.3 Paper Structure

Section 2 begins with a concise overview of QECCs, followed by a detailed description of the eight QECCs utilized in this study. Section 3 introduces the eight benchmarking parameters, delves into the criteria for selecting codes & parameters, and outlines the methodology for comparative analysis. Section 4 presents an in-depth analysis of the eight QECCs in relation to the chosen parameters. Section 5 discusses prospective future work and challenges. Finally, the paper concludes in Section 6.

## 2 Theoretical Background

This section gives a general overview of the quantum error correction codes and then moves on to describe the codes that have been considered in this study.

### 2.1 Brief Overview of QECCs

#### 2.1.1 Error Correction in Quantum Systems

Quantum Error-Correcting Codes (QECCs) differ fundamentally from classical error correction

as they manage information encoded in quantum states, characterized by properties like superposition and entanglement [51]. Quantum systems are notably sensitive, with quantum states being easily disrupted by external disturbances [56]. This fragility presents a significant hurdle for reliable quantum computation and information storage, effectively addressed by QECCs [32].

QECCs function by encoding quantum information across multiple qubits, allowing the system to detect and correct errors without directly measuring the quantum state, in compliance with the no-cloning theorem [78, 24]. Quantum errors primarily include bit-flip and phase-flip errors, with more complex errors combining these two [64]. QECCs correct these errors through entangled states and collective measurements [13].

#### 2.1.2 Code Varieties and Applications

Various QECCs have been proposed: Shor Code, the first QECC capable of correcting arbitrary single-qubit errors [64]; Steane Code, a Calderbank-Shor-Steane (CSS) code illustrating fault-tolerant quantum computation principles [66]; Topological Codes, like Kitaev's Toric code, using a lattice of qubits for robustness against local errors [41] and Surface Codes, known for simpler error correction procedures, suitable for large-scale quantum computations [28].

QECCs are integral to practical quantum computing, particularly in achieving fault-tolerant quantum computation, a vital step for scalable and reliable quantum computers [3]. Ongoing research in QECCs focuses on optimizing code efficiency, reducing qubit overhead, and enhancing fault tolerance, crucial for the evolution of quantum computing [72].

### 2.2 Descriptions of QECCs Under Study

#### 2.2.1 Repetition Code

The Quantum Repetition Code [23, 55] is one of the simplest forms of QECCs. Its primary function is to protect quantum information against errors, particularly bit-flip errors. This code extends the concept of the classical repetition code into the quantum realm, leveraging the fundamental principles of quantum mechanics [17]. The quantum repetition code works by encoding a single qubit of information across multiple qubits. For instance, in a 3-qubit repetition code,

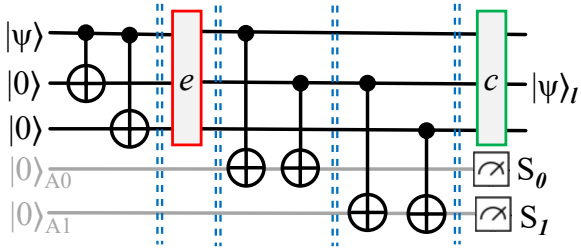


Figure 1: **Quantum circuit implementing a 3-qubit repetition code:** It features a state preparation circuit, the possibility of a single bit-flip error on any of the three qubits, two ancilla qubits initialized to  $|0\rangle$  for parity checking, a first stabilizer circuit ( $Z \otimes Z \otimes I$ ) for measuring parity between the first two qubits, a second stabilizer circuit ( $I \otimes Z \otimes Z$ ) for the last two qubits, and syndrome bits  $S_0, S_1$  obtained via the ancilla qubits for error detection and deduction. Correction is achieved by applying a sequence of self-inverse Pauli-gates ( $c$ ) to the qubit requiring correction.

a single logical qubit  $|0\rangle$  or  $|1\rangle$  is encoded as  $|000\rangle$  or  $|111\rangle$ , respectively. This redundancy allows the code to detect and correct bit-flip errors that might occur on individual qubits.

Error detection in the quantum repetition code is accomplished through a process known as syndrome measurement. This involves measuring the parity of neighboring qubits without collapsing the overall quantum state. For example, if the encoded state is  $|000\rangle$  and a bit-flip error occurs on the second qubit, the state changes to  $|010\rangle$ . The syndrome measurement detects this error by noticing the changed parity between the first and second qubits and the second and third qubits. Once detected, quantum operations can be applied to correct the error and restore the original state. Fig. 1 shows a quantum circuit for a 3-qubit repetition code, featuring state preparation, potential single bit-flip error detection, parity checking with two ancilla qubits, and error correction using self-inverse Pauli-gates.

### 2.2.2 Shor Code

The Shor Code [64], named after its inventor Peter Shor, is a landmark in the field of quantum error correction. Introduced in 1995, it was the first quantum error-correcting code (QECC) that demonstrated the feasibility of correcting arbitrary quantum errors, specifically both bit-flip and phase-flip errors, in a quantum bit or qubit.

The Shor Code encodes a single qubit of quantum information into a highly entangled state of

nine physical qubits. This 9-qubit code is effectively a combination of the classical 3-bit repetition code, which corrects bit-flip errors, and the quantum phase-flip code, which corrects phase-flip errors.

The Shor Code utilizes a specific arrangement: The first layer of encoding replicates the qubit three times, preparing for bit-flip error correction and the second layer encodes each of these three qubits into three more qubits to guard against phase-flip errors. This two-layer structure makes the Shor Code capable of correcting any single-qubit error, whether it is a bit-flip, a phase-flip, or a combination of both on any of the nine qubits. It is described as a degenerate code, where different error types can affect the codewords similarly. The two basis states of the code are represented as  $|0_L\rangle$  and  $|1_L\rangle$ , intricately constructed from the superposition and entanglement of the nine qubits. The two basis states for the code are defined as:  $|0_L\rangle = \frac{1}{\sqrt{8}}(|000\rangle + |111\rangle)(|000\rangle + |111\rangle)(|000\rangle + |111\rangle)$  and  $|1_L\rangle = \frac{1}{\sqrt{8}}(|000\rangle - |111\rangle)(|000\rangle - |111\rangle)(|000\rangle - |111\rangle)$ . This structure ensures that the Shor Code can correct a single X error in any one block of three qubits and a single Z error on any of the nine qubits, classifying it as a full quantum error-correcting code

In the Shor Code, X errors are detected and corrected by using a correction circuit similar to that in the three-qubit code, applied to each block of three qubits. The process involves identifying single bit-flip errors and rectifying them accordingly. For phase-flip errors, the correction is achieved by examining the sign differences between the three blocks. This is executed using a set of six CNOT gates that compare the signs of blocks one and two, followed by another set of CNOT gates for blocks two and three. The unique aspect of the Shor Code is its degeneracy - a phase flip on any one qubit in a block of three has the same effect, hence, knowing the block in which the error occurs is sufficient to apply the correction operator. The Shor Code can correct for up to three individual bit flips provided each occurs in a different block of three. However, it is typically considered a single error-correcting code as it cannot handle multiple errors if they occur in specific locations. Fig. 2 depicts the encoding, error introduction, and error correction of a 9-qubit Shor code.

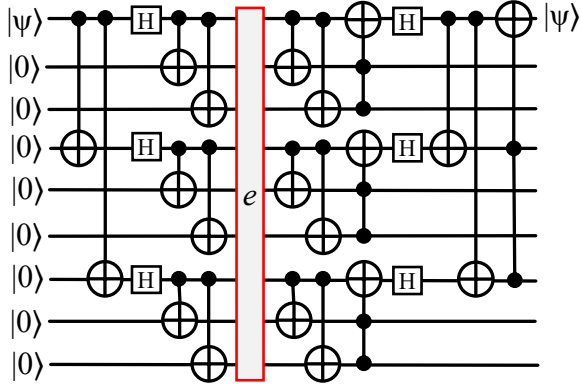


Figure 2: **Quantum circuit implementing a 9-qubit Shor code:** It features a state preparation encoding circuit, the possibility of a single bit-flip or phase flip error on any of the three qubits, error correction, and error recovery.

### 2.2.3 Steane Code

The Steane Code [65], also known as the 7-qubit code, was introduced by Andrew Steane in 1996 as a part of the Calderbank-Shor-Steane (CSS) [13, 66] family of quantum error-correcting codes. It represents a significant advancement in the field of quantum error correction, offering a symmetrical approach to correcting both bit-flip and phase-flip errors. The Steane Code encodes a single logical qubit into seven physical qubits. It is based on classical error-correcting codes, specifically the [7,4,3] Hamming code, which corrects single-bit errors in classical computing. In the quantum realm, this code is extended to correct both bit-flip and phase-flip errors in quantum bits. The key feature of the Steane Code is its CSS construction, which allows separate correction of bit-flip and phase-flip errors. This separation simplifies the error correction process and reduces the complexity of quantum circuits needed for implementation. The logical zero  $|0_L\rangle$  and one  $|1_L\rangle$  states in the Steane Code are defined using superpositions of the Hamming code's even and odd weight codewords, respectively.

The Steane Code employs syndrome measurements for error detection, which uniquely indicate the presence and type of error without collapsing the quantum state. This code is comprised of 6 stabilizer generators:  $IIIXXXX$ ,  $IXXIIXX$ ,  $XIXIXIX$ ,  $IIIZZZZ$ ,  $IZZIIZZ$  and  $ZIZIZIZ$ . Due to this structure, the Steane Code can independently correct X and Z errors using separate circuits. This dual capability is

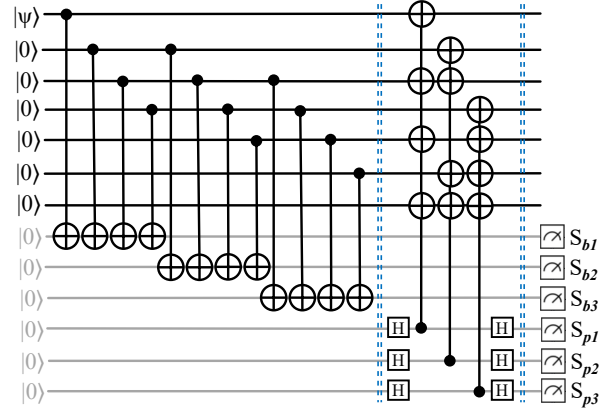


Figure 3: **Implementing a 7-qubit Steane code decoding circuit:** It features three bit-flip detection stabilizers and three phase-flip detection stabilizers along with six ancilla qubits and their respective syndrome measurements (3 for detecting bit-flips and 3 for detecting phase-flips.)

central to its functionality, allowing for the efficient correction of single-qubit errors in quantum systems. The logical  $|0\rangle$  and  $|1\rangle$  states of this code are:  $|0_L\rangle = \frac{1}{\sqrt{8}}(|0000000\rangle + |1010101\rangle + |0110011\rangle + |1100110\rangle + |0001111\rangle + |1011010\rangle + |0111100\rangle + |1101001\rangle)$  and  $|1_L\rangle = X_L|0_L\rangle$ ; where  $X_L = XXXXXX$ . Fig. 3 depicts the error-detecting circuit of the 7-qubit Steane code.

### 2.2.4 Toric Code

The Toric Code [40], introduced by Alexei Kitaev, represents a novel approach to quantum error correction by leveraging topological properties. Its use of a two-dimensional lattice structure is unique, making it resistant to a broad class of local errors.

In the Toric Code, qubits are placed on the edges of a two-dimensional lattice on a torus. The topology of the lattice defines logical qubits and error correction is achieved by measuring vertex and plaquette operators. These operators are defined as: Vertex operators:  $O_v = \prod_{i \in v} X_i$  and Plaquette operators:  $O_p = \prod_{i \in p} Z_i$ . In these expressions,  $X_i$  and  $Z_i$  represent Pauli X and Z operators applied to the qubits. The products are taken over qubits around a vertex  $v$  for vertex operators, and around a plaquette  $p$  for plaquette operators.

Errors in the Toric Code manifest as excitations in this lattice structure. Bit-flip errors disrupt vertex operators, while phase-flip errors dis-

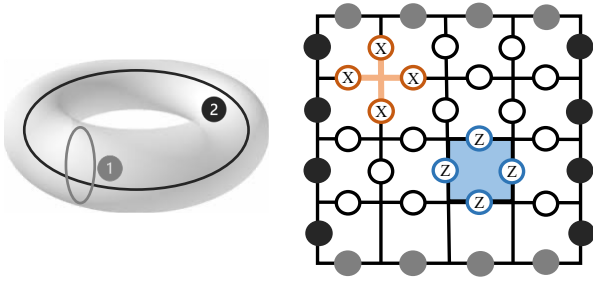


Figure 4: **Representation of a toric code:** The torus on the left shows two rings. Its corresponding lattice on the right is arranged to reflect these rings, with top-bottom and left-right lattice qubits being identical. The X-stabilizer (vertex operator), marked in orange, acts on four 'X' labeled qubits to detect Z errors. Conversely, the Z-stabilizer (plaquette operator), highlighted in blue, operates on four 'Z' labeled qubits, enabling the detection of X errors on any of these qubits.

rupt plaquette operators. The code detects errors by checking for these excitations. The topological nature of the code allows for the identification and correction of errors based on the collective state of multiple qubits, rather than individual qubit states. Fig. 4 represents the toric code and the acting of the X and Z stabilizers on its unique lattice structure.

### 2.2.5 Surface Code

Surface Codes [22] are a class of quantum error-correcting codes that extend the principles of the Toric Code to a planar geometry, meaning it is not modeled around a torus. They are known for their high threshold error rate, making them a promising candidate for scalable quantum computation.

Surface codes, similar to toric codes in stabilizers and error detection, have two main layouts: unrotated [28] and rotated [73]. Unrotated surface codes use a square lattice, with data qubits on square edges, Z-stabilizers on surfaces, and X-stabilizers at vertices. Rotated surface codes feature a tilted lattice, with X and Z stabilizers alternating in a chessboard pattern. The difference in lattice arrangement impacts their error-correction efficiency, with rotated codes generally preferred for long-distance QEC due to a higher error threshold and simpler implementation.

Error detection in Surface Codes is accomplished through the measurement of these stabilizer operators. A non-trivial measurement outcome (eigenvalue -1) indicates an error. The pla-

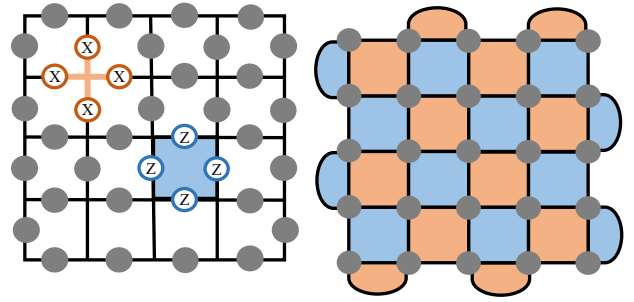


Figure 5: **Layouts of a surface code:** The lattice on the left shows an unrotated surface code which is similar to a toric code except that it is planar and is not modeled around a torus. The lattice on the right shows a rotated surface code where alternating surfaces form X and Z stabilizers.

nar nature of Surface Codes facilitates the implementation of fault-tolerant gate operations and scalable quantum computing architectures. Fig. 5 shows the two different layouts of a surface code: unrotated and rotated.

### 2.2.6 Bacon-Shor Code

The Bacon-Shor Code [6, 64] is a type of quantum error-correcting code that simplifies error correction in quantum computing. It is a subclass of the more general family of Shor codes.

The Bacon-Shor codes are stabilized over a square lattice, where the lattice dimensions dictate the X and Z error correction properties. The size of the lattice determines the total number of errors the code can correct. Such a code is defined as an  $m_1 \times m_2$  lattice of qubits and is symmetric when  $m_1 = m_2$ . The X and Z stabilizers act on all qubits present on adjacent columns and rows respectively. If  $O_{i,j}$  is an operator acting on the qubit at the position  $(i, j)$ , which  $i \in \{0, 1, \dots, m_1 - 1\}$  and  $j \in \{0, 1, \dots, m_2 - 1\}$ . The code stabilizer group is given by:  $S = \langle X_{i,*} X_{i+1,*}, Z_{*,j} Z_{*,j+1} \rangle$ , with generators expressed as a product of adjacent neighbor 2-qubit operators:  $X_{i,*} X_{i+1,*} = \bigotimes_{k=0}^{m_2-1} X_{i,k} X_{i+1,k}$  and  $Z_{*,j} Z_{*,j+1} = \bigotimes_{k=0}^{m_1-1} Z_{k,j} Z_{k,j+1}$ .

Syndrome extraction is done by measuring these operators, which are local and are on fewer qubits. The shortest Bacon-Shor code is  $[[9, 1, 3, 3]]$  with four stabilizer generators:  $XXXXXXIII$ ,  $IIIXXXXXX$ ,  $ZZIZZIZZI$  and  $IZZIZZIZZ$ . Fig. 6 depicts the encoding and stabilizer measurement in Bacon-Shor code [68, 23].

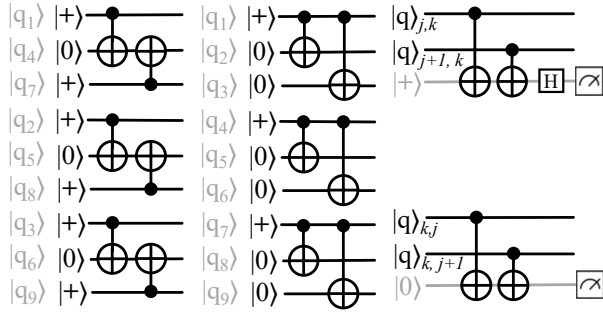


Figure 6: **Encoding and measurement in Bacon-Shor code:** The first two circuits show the encoding of logical  $|0\rangle$  and  $|+\rangle$  respectively for a  $3 \times 3$  representation. The last two circuits show the measurement of operators  $X_{j,k} X_{j+1,k}$  and  $Z_{k,j} Z_{k,j+1}$  respectively with one ancilla qubits.

### 2.2.7 3D Color Code

The quantum color code [11], another form of topological QECC, takes a unique approach to error detection and correction. It extends the principles of surface codes by encoding logical qubits into a three-dimensional structure, often visualized as a two-dimensional lattice with ‘colors’ for ease of interpretation [43, 14]. There exist numerous two-dimensional renditions of a color code, among which we have chosen to utilize a representation in the form of a triangulated lattice filled with hexagonal surfaces for this discussion. Within this chosen format, each vertex signifies a logical qubit, while each hexagonal face corresponds to a stabilizer. However, color codes introduce a third type of stabilizer. In color codes, each hexagon in the lattice represents a different type of stabilizer: X-type, Z-type, and Y-type stabilizers. The Y-type stabilizer is associated with errors that involve both a bit-flip and a phase-flip simultaneously, thus accounting for its 3D structure. What sets color codes apart is their ability to detect and correct a broader range of errors. While surface codes can correct any single quantum error, theoretically color codes can handle more complex error models, including certain correlated or coherent errors. Fig. 7 showcases two distinct instances of color codes, each progressively larger as they scale according to distance. These color codes, while fundamentally three-dimensional, are depicted here within a two-dimensional triangular lattice format with hexagonal faces for ease of representation. The logical qubits composing the logical

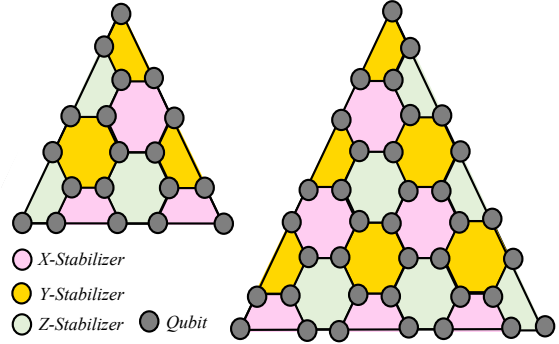


Figure 7: **Illustration of two distinct iterations of color codes, each enlarging proportionally with distance.** Though intrinsically three-dimensional, color codes are rendered here within a two - dimensional triangular lattice format encompassing hexagonal surfaces for simplified visual interpretation. The logical qubits, integral components of the logical state, are marked as gray-blobs. Each hexagonal surface is associated with a stabilizer, a key element for error detection and correction. Z-stabilizers are denoted by pink - hexagons, while the green - hexagons correspond to X-stabilizers. Color codes, distinguishing themselves from surface codes, incorporate an additional type of stabilizer, the Y-stabilizer, depicted by the yellow - hexagons.

state are represented as gray-blobs. Each hexagonal face corresponds to a stabilizer, crucial to error detection and correction. Pink - hexagons denote Z-stabilizers, while the green - hexagons signify X-stabilizers. Differing from surface codes, color codes possess an additional stabilizer type, the Y-stabilizer, represented here by the yellow - hexagons.

3D Color Codes are capable of correcting a wider range of errors compared to their 2D counterparts. The introduction of an additional spatial dimension allows for more complex and robust error correction strategies. They can correct any arbitrary single-qubit error within their lattice structure and are particularly adept at dealing with correlated errors, which are a significant challenge in quantum computing.

Fig. 7 illustrates two iterations of color codes within a two-dimensional triangular lattice, simplifying their inherent three-dimensional structure. The diagram features logical qubits as gray blobs, surrounded by hexagonal stabilizers crucial for error detection and correction: pink hexagons for Z-stabilizers, green for X-stabilizers, and uniquely for color codes, yellow hexagons representing Y-stabilizers. This visual representa-

tion highlights the complex interplay and scalability of stabilizers in color codes, crucial for advanced quantum error correction.

### 2.2.8 Heavy Hexagon Code

Heavy hexagon codes [15] are a type of quantum error-correcting code that utilizes a lattice structure resembling a hexagon. They are designed to protect quantum information against errors more efficiently than some other quantum codes due to their unique geometric arrangement of qubits.

The heavy hexagon lattice is constructed by augmenting a hexagonal lattice with additional qubits placed at strategic locations. These additional ‘heavy’ qubits increase the code’s tolerance to errors by enhancing the connectivity between qubits, which is essential for the syndrome measurement process in error correction. The code’s error correction mechanism is designed to detect and correct both bit-flip (X) and phase-flip (Z) errors. It does so through a series of syndrome measurements that diagnose the type and location of the errors, allowing for targeted correction that preserves the fidelity of the quantum state.

This lattice stabilizer subsystem code synthesizes elements from both Bacon-Shor and surface-code frameworks, and encodes a single logical qubit into  $n = \frac{5d^2 - 2d - 1}{2}$  physical qubits where  $d$  denotes the code distance. This lattice is characterized by its sparse connectivity, typically not exceeding three connections per qubit, making it a robust candidate for systems with fixed-frequency transmon qubits that are vulnerable to frequency collision errors.

On this lattice, data qubits and ancillas are strategically distributed along the hexagonal vertices and edges. A designated subset of these ancilla qubits serves as flag qubits, crucial for the detection of high-weight errors that may result from a limited number of fault events. The stabilizers tasked with the detection of X-type errors are constituted by the product of weight-two Z-type gauge operators, which collectively form the surface code stabilizers. Meanwhile, the X-type stabilizers, reminiscent of columnar operators in the Bacon-Shor code, are deduced by aggregating products of weight-four and weight-two X-type gauge operators. Fig. 8 represents the layout and stabilizer circuits of a heavy-hexagon code.

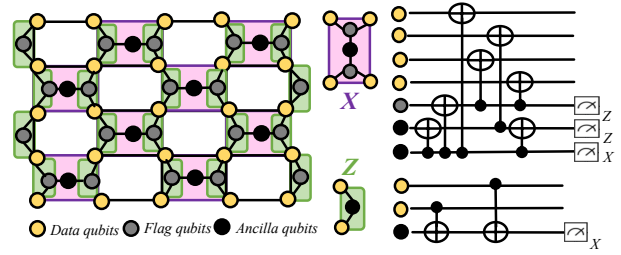


Figure 8: **Representation and stabilizer circuits of a heavy-hexagon code.** The left of the figure is the actual layout of a distance = 5 heavy-hexagon code. The right of the figure contains two circuits to perform the X and Z parity checks respectively.

## 3 Benchmarking Methodology

This section outlines the benchmarking parameters, explains the rationale behind the selection of codes & parameters, and discusses the methodology used for comparative analysis.

### 3.1 Explanation of Benchmarking Parameters

#### 3.1.1 Qubit Overhead

Qubit Overhead is a fundamental parameter in assessing the efficiency of a QECC. It refers to the number of physical qubits needed to encode a logical qubit; lower overhead is preferable as it implies fewer resources for error correction. However, this must be balanced against the code’s ability to correct errors, which often requires more qubits for increased distance. Therefore, analyzing the trade-off between qubit overhead and error correction capabilities is crucial in evaluating the practicality of a QECC.

#### 3.1.2 Error Threshold

The Error Threshold is a critical benchmark for the robustness of a quantum error correction code. It represents the maximum physical error rate under which a QECC can effectively correct errors. A higher threshold indicates a more fault-tolerant code, making it more desirable for practical quantum computing where error rates are non-negligible.

#### 3.1.3 Error Protection

Error Protection capability is the measure of a QECC’s ability to identify and correct a range of quantum errors, including bit flips, phase flips,

and their combinations (Pauli errors). The ultimate goal is to design QECCs capable of detecting and correcting all possible quantum errors. A QECC's versatility in handling diverse error types is a significant indicator of its effectiveness and practical utility in quantum computing environments.

### 3.1.4 Decoding

The availability and efficiency of Decoding Algorithms are essential for the practical implementation of QECCs. Decoding is the process of interpreting syndrome measurements to identify and correct errors. The more decoding algorithms a QECC is compatible with, the more flexible and adaptable it is. The performance of a QECC is heavily reliant on the efficiency of these algorithms, which should be fast and accurate to maintain the integrity of quantum information.

### 3.1.5 Transversal Gates

Transversal Gates play a crucial role in the implementation of quantum error correction. They facilitate operations on encoded qubits without decoding them, thereby preserving the error correction capability. The complexity and type of transversal gates that a QECC supports can significantly affect its functionality and integration with quantum circuits. Advanced techniques like lattice surgery, while complex, offer enhanced capabilities in error correction and logical operations, marking an important consideration in QECC design.

### 3.1.6 Scalability

Scalability is an essential factor for the practical application of QECCs in large-scale quantum computing. It refers to a QECC's ability to maintain its error correction effectiveness as the system size increases or as it operates in environments with higher levels of noise. Scalability is crucial for the advancement of quantum computing, as it determines whether a QECC can be effectively used in more complex and realistic quantum systems.

### 3.1.7 Realization

The Realization of a QECC across different qubit types is a testament to its adaptability and prac-

tical relevance. The versatility of a QECC in being implemented with various qubit technologies (such as superconducting qubits, trapped ions, etc.) is vital for its applicability in diverse quantum computing architectures. This parameter is a strong indicator of a QECC's potential for widespread adoption in the quantum computing field.

### 3.1.8 Complexity

The Structural and Operational Complexity of a QECC impacts its implementability and efficiency. This encompasses the intricacy of its encoding, error detection, and correction processes. A less complex QECC might be easier to implement but may offer limited error correction capabilities. Conversely, a more complex QECC might provide robust error correction but at the cost of increased resource demands and operational challenges. Balancing complexity with effectiveness and resource efficiency is key in the design and selection of QECCs for practical quantum computing.

## 3.2 Criteria for Selection of Codes and Parameters

The eight chosen quantum error correction codes illustrate the historical and conceptual evolution of QECCs. Starting from basic concepts like the quantum repetition code to more complex structures like the heavy-hexagon code, they form a kind of 'family tree' that shows the development and diversification of QECCs over time. They encompass a wide array of error correction strategies, from simple error correction (quantum repetition code) to sophisticated techniques like those used in the surface and color codes. This diversity ensures a comprehensive understanding of different error correction methodologies. They vary significantly in terms of complexity and scalability. For example, the Shor code and Steane code represent more traditional approaches, whereas the toric and surface codes are geared toward large-scale quantum computing. This range allows for the assessment of QECCs across different scalability requirements. Different codes are optimized for different error models. Including a variety of codes ensures that your benchmarking study addresses a wide range of error scenarios. Some codes, like the surface code, are

designed with practical implementation in mind, considering current quantum computing limitations. This inclusion allows for an assessment of QECCs not just in theory but also in their practical realization. The selection spans codes with varying qubit overheads. For instance, the quantum repetition code is simple but not efficient, whereas codes like the toric code aim to balance error correction efficacy with resource efficiency. These eight codes collectively cover the spectrum of QECCs, from basic to advanced, from theoretical to practical. This range is crucial for a comprehensive benchmarking study. While there are other QECCs, including more might lead to redundancy without significantly adding to the understanding of QECC performance. The chosen codes are sufficiently representative of the broader field. This selection allows for a comparative analysis that can highlight the strengths and weaknesses of different approaches to quantum error correction. It enables a holistic view of the current state of QECC technology.

The eight selected parameters encompass all critical dimensions of QECC functionality - from basic resource requirements (like qubit overhead) to advanced operational aspects (like error protection and decoding). This wide-ranging coverage ensures no key aspect of QECC performance is overlooked. They strike a balance between the efficiency of a QECC (in terms of resource utilization and complexity) and its robustness (error threshold and protection capabilities). This balance is crucial for practical quantum computing where resources are limited and error rates are non-negligible. Parameters such as scalability and realization reflect the real-world challenges of implementing QECCs in various quantum computing environments. They ensure that the assessment of QECCs goes beyond theoretical effectiveness to include practical viability. Each parameter addresses a distinct aspect of QECC performance. There is minimal overlap between them, ensuring that each provides unique and valuable insight into the QECC's capabilities. While these parameters are comprehensive based on the current understanding and needs of quantum computing, they also allow for flexibility. As quantum technology evolves, these criteria can be adapted or expanded to include new developments and requirements. Having a set of widely accepted parameters aids in standardizing the as-

essment of QECCs. This standardization is crucial for comparative analysis and for guiding improvements in QECC designs.

### 3.3 Approach to Comparative Analysis

The primary objective of this comparative analysis is to establish a comprehensive benchmark for QECCs. This benchmark serves as a reference point for future developments in QECCs, guiding researchers and practitioners in evaluating new codes against established parameters. The analysis acknowledges that the 'best' QECC depends on specific operational contexts, such as the number of qubits available, the type of errors prevalent in the system, and the practical constraints of quantum computing environments.

Each selected QECC will be evaluated based on predefined criteria, including qubit overhead, error threshold, error protection, decoding, transversal gates, scalability, realization, and complexity. This structured approach ensures a comprehensive and uniform assessment of each code's capabilities and limitations.

The analysis aims to highlight that while no single QECC is universally superior, each has its strengths and weaknesses. Through this structured and comprehensive approach to comparative analysis, the study will provide valuable insights into the relative merits of different QECCs. It will aid in the development of more effective, efficient, and contextually appropriate QECCs, thereby advancing the field of quantum computing. The ultimate goal is to foster an environment where QECC selection is based on an informed, nuanced understanding of each code's performance in relation to specific operational needs and constraints.

## 4 Benchmarking Analysis

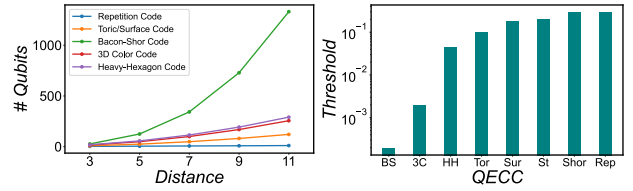
This section begins by examining the performance of eight distinct QECCs against a set of eight benchmarking parameters. It then progresses to discuss the significance of benchmarking variations within existing QECCs, emphasizing the importance of such assessments.

### 4.1 Comparative Benchmarking of QECCs

Table 1 shows the parameter analysis for all quantum error correction codes used in this study.

Table 1: Parameter Analysis for QECCs.

Parameters	Quantum Repetition Code	Shor Code	Steane Code	Toric Code	Surface Code	Bacon-Shor Code	3D Color Code	Heavy-Hexagon Code
<b>Qubit Overhead</b>	$d$	9	7	$d^2$	$d^2$	$d^3$	$\frac{(3d-1)^2}{4}$	$\frac{(5d^2-2d-1)}{2}$
<b>Error Threshold</b>	0.3	0.3	0.2	0.01	0.018	0.00194	0.002	0.045
<b>Error Protection</b>	Only half of all bit flip errors.	Two qubits, all error type	Detects errors on 2 qubits, corrects 1	All Pauli errors	All Pauli errors	All Pauli errors	All Pauli errors	All Pauli errors
<b>Decoding</b>	Automation, ML	CNOT/ H Gates	CNOT/ H Gates	MWPM, Tensor, 10+ Algo	MWPM, Tensor, 10+ Algo	Statistical Mapping, Check operators	Restriction, MaxSAT, 3+ Algo	MWPM, ML, Neural Network, 3+ Algo
<b>Transversal Gates</b>	None	None	Clifford Gates	TPG/Lattice Surgery	Lattice Surgery	Teleportation	Lattice Surgery	Lattice Surgery
<b>Scalability</b>	No	No	No	Yes	Yes	Yes	Yes	Yes
<b>Realization</b>	Superconducting, Trapped ion, etc	Trapped ion, Optical systems	Trapped ion, Rydberg atom	Superconducting, Rydberg atom arrays	Superconducting, Rydberg atom arrays, Ising anyons	Trapped ion	None	Superconducting
<b>Complexity</b>	Very Low	Low	Low	Very High	High	Medium	Extremely High	Extremely High


 Figure 9: **Qubit overhead and threshold analysis.** The left of the figure shows the increase in the number of qubits with distance. The right of the figure shows the threshold error rate of various QECCs.

In terms of qubit overhead, it is expressed as a function of the distance variable,  $d$ . Specifically, the Shor and Steane codes have fixed qubit overheads of 9 and 7, respectively. The repetition code's overhead increases linearly with  $d$ . The overhead for the toric and surface codes grows at a rate proportional to  $d^2$ , while for the Bacon-Shor code, it escalates in proportion to  $d^3$ . The 3D color code and the heavy-hexagon code exhibit qubit overheads of  $\frac{(3d-1)^2}{4}$  and  $\frac{5d^2-2d-1}{4}$ , respectively. Figure 9 (left) illustrates the rise in the number of qubits corresponding to increasing values of  $d$ . For instance, a Bacon-Shor code at distance 11 demands over 1000 qubits, highlighting the significance of qubit overhead as a key benchmarking metric.

The threshold error rate is a critical metric for quantum error correction codes (QECCs), indicating the highest level of physical errors they can effectively correct. This makes it a key consideration in evaluating the performance of QECCs. The threshold error rates for various codes like the repetition, Shor, Steane, toric, surface, Bacon-Shor, 3D color, and heavy-hexagon codes are  $3.0 \times 10^{-1}$  [16],  $3.0 \times 10^{-1}$  [64],  $2.0 \times 10^{-1}$  [66],  $1.0 \times 10^{-2}$  [40],  $1.8 \times 10^{-2}$  [16, 36],  $1.9 \times 10^{-3}$  [5],  $2.0 \times 10^{-2}$  [14] and  $5.0 \times 10^{-2}$  [8] respectively, as depicted in Fig. 9 (right). While the repetition code exhibits the highest threshold, it is important to note its limitation to only detecting bit-flip errors, rendering it impractical for broader applications. Thus, finding a balance in these characteristics is crucial for effective quantum error correction.

Different QECCs have different types and ranges of errors they can correct. The repetition code detects bit flip errors on  $\lfloor (n-1)/2 \rfloor$  qubits but does not detect any phase-flip errors [59]. Conversely, the Shor code detects two-qubit errors or corrects an arbitrary single-qubit error

[64]. The Steane code is a distance 3 code, detecting errors on 2 qubits and correcting errors on 1 qubit [66]. More complex codes like the toric, surface, 3D color, and heavy-hexagon codes can detect and correct all Pauli errors. However, their effectiveness depends on the code's distance, which is directly related to the qubit overhead and the complexity of implementation. The toric code on a  $d \times d$  torus is a  $[[2L^2, 2, L]]$  code, encoding two qubits, while the surface code is a  $[[L^2 + (L - 1)^2, 1, L]]$  code, encoding only one qubit [29]. The Bacon-Shor code variant,  $[[m_1 m_2, 1, \min(m_1, m_2)]]$  code, has a distance  $d = \min(m_1, m_2)$  [6]. Unlike the surface code, the color code can suffer from unremovable hook errors due to the specifics of its syndrome extraction circuits, requiring fault-tolerant decoders to use additional flag qubits [10]. In contrast, the heavy-hexagon code is an example of the Bacon-Shor type stabilizer [15].

A decoding algorithm is essential for interpreting stabilizer syndrome values to identify the type and location of errors in a quantum error correction code (QECC). These algorithms introduce additional complexity to QECCs, and the performance of these codes is highly dependent on such algorithms. The availability of multiple decoding algorithms enhances the versatility of a code. The repetition code can use classical 2D Ising model decoders [74] or machine learning-based approaches [20]. The Shor and Steane codes employ CNOT and Hadamard gates for decoding [49]. The toric and surface codes are supported by a variety of decoding algorithms, including minimum weight perfect-matching (MWPM) [27], tensor decoders [12], union-find decoders [21], brief perfect matching [37], renormalization group methods [25], Markov-chain Monte Carlo techniques [39], cellular automata [34], neural networks [75], sliding and parallel window decoders [71], generalized belief propagation [53], among others. The Bacon-Shor code uses the mapping effect of noise to statistical mechanical models for decoding [61]. Although its check operators are few-body, stabilizer weights scale with the number of qubits, and stabilizer expectation values are obtained by taking products of gauge-operator expectation values [35]. The 3D color code may utilize various decoders such as the projection decoder [44], integer-program-based decoder [67], restriction decoder [14], cellular-

automation decoder [60], or the MaxSAT-based decoder [7].

Transversal gates facilitate operations on logically encoded qubits without the need for decoding. The choice of transversal gate contributes to the complexity of implementing a QECC. The repetition and Shor codes do not rely on transversal gates and are infrequently scalable across multiple qubits. The Steane code employs single-qubit Clifford gates, realizing the binary octahedral subgroup [81]. The toric, surface, 3D color, and heavy-hexagon codes utilize lattice surgery [38]. In the toric code, transversal Pauli gates can be applied to non-trivial loops [48]. In symmetric Bacon-Shor codes, the Logical Hadamard is transversal up to a qubit permutation and can be implemented via teleportation [83].

The practical implementations of QECCs reflect their applicability in real-world scenarios, and the range of qubit technologies they can be implemented on indicates their versatility. The repetition code has been realized on superconducting qubits [57, 1], trapped-ion qubits [18], liquid-state NMR [82], and NV diamond qubits [77]. The Shor code has seen implementation on trapped-ion qubits [50] and in optical systems [46]. The Steane code has been realized with trapped-ion qubits [52] and Rydberg atom arrays [9]. Both the toric and surface codes have been implemented using Ising anyons [80], while the surface code has also been realized with superconducting qubits [63] and Rydberg atomic arrays [9]. The Bacon-Shor code's realization has been limited to trapped-ion qubits [26]. As of now, there has been no practical realization of the 3D color code. The heavy-hexagon code has been implemented in superconducting qubits [70].

The repetition, Shor, and Steane codes are not scalable across multiple qubits, in contrast to the toric, surface, Bacon-Shor, 3D color, and heavy-hexagon codes, which are scalable. The implementation complexity of these codes can be gauged from their circuit or lattice structures. The repetition code has a very low complexity. The Shor and Steane codes can be categorized as having low complexity. The surface code, with its square lattice structure, is considered highly complex. Similarly, the toric code, despite its resemblance in structure, is deemed highly complex due to its encoding of two qubits instead of one. The Bacon-Shor code falls into the medium com-

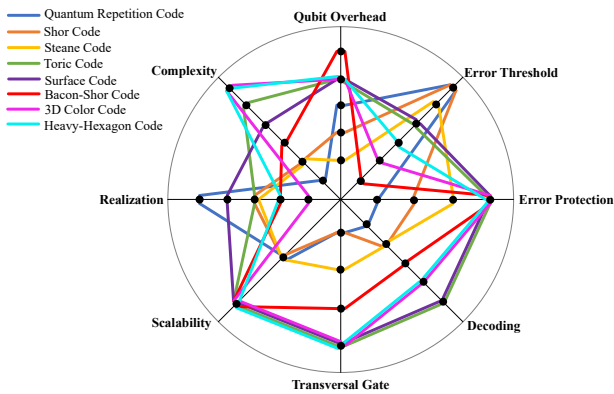


Figure 10: **Radar chart representing comparative analysis of eight QECCs across eight parameters.** The parameter axes radiating from the center are as follows: Qubit Overhead =  $\{7, 9, d, d^2, d^3\}$ ; Error Threshold =  $\{10^{-4}, 0.002, 0.045, 0.1, 0.2, 0.3\}$ ; Error Protection =  $\{\text{bit-flip, two-qubit errors, detect two-qubit errors or corrects one, all Pauli errors}\}$ ; Decoding =  $\{\text{classical, CNOT/H, 2, 5, 10+}\}$ ; Transversal Gates =  $\{\text{none, Clifford, teleportation, lattice surgery}\}$ ; Scalability =  $\{\text{no, yes}\}$ ; and Realization =  $\{\text{none, 1, 2, 3, 6}\}$ .

plexity category. Finally, the lattice structures of the 3D color and heavy-hexagon codes indicate their extremely high complexity in terms of implementation.

Now that we have analyzed QECCs in terms of their parameters, we can collectively benchmark them using a radar chart as shown in Fig. 10. This chart consists of eight axes, each representing a different parameter. Colored lines connecting the axes represent the QECCs. The ‘qubit overhead’ parameter in the chart varies from constants to the highest order  $d^3$ . The ‘error threshold’ spans from the lowest to the highest order value. ‘Error protection’ encompasses types ranging from basic bit-flip to all Pauli errors. ‘Decoding’ varies from a single classical decoder to the maximum number available for any QECC. ‘Transversal gates’ extend from none to the most complex, lattice surgery. ‘Scalability’ is binary, indicated by yes or no. ‘Realization’ varies from none to the maximum number of qubit technologies on which a QECC has been implemented. The ‘complexity’ of a QECC is rated on a scale of six levels, from very low to extremely high.

Considering the surface codes and comparing them with the radar chart in Fig. 10, we observe that they offer the highest form of error protection with scalability and have been realized on a considerable number of qubit technologies,

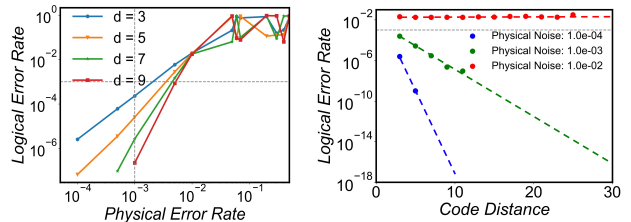


Figure 11: **Analysis of logical error rates in surface codes.** On the left, the image demonstrates how higher distance codes result in lower logical error rates for a specific physical error rate. The right side of the image illustrates the necessary increase in code distance to achieve desired logical error rate goals under different physical error rates.

with multiple decoders available. Despite having a relatively good error threshold, making them a viable option, they come at the cost of high qubit overhead, complex implementation, and the need to utilize the most complex transversal gate. Conversely, the repetition code features the least complex transversal gate and is straightforward to implement, but offers limited error protection. The choice of QECC thus becomes an art of balancing parameters and requirements.

## 4.2 Benchmarking QECC Variations

It is important to understand that the radar chart presented earlier highlights only the general comparative differences among various codes. We will now focus on surface codes, which are highly applicable in real-world scenarios. For illustration, let’s consider surface codes with distances of 3, 5, 7, and 9. Despite sharing common features like an identical error threshold, the same transversal gates, and equal access to decoding algorithms, these codes exhibit distinctions in several parameters. The structure of a surface code is a  $d \times d$  lattice, meaning the qubit overhead increases as the distance grows. All surface codes offer comparable error protection, which is enhanced with greater distances. Figure 11 (left) depicts the achievable logical error rates for varying physical error rates across different surface code distances. At a given physical error rate, a larger distance code yields a lower logical error rate. Moreover, all surface codes are scalable, but as the physical error rate rises, the necessity for greater distances becomes apparent. Although scalability is maintained with larger distances, it presents greater challenges. Figure 11 (right) illustrates the re-

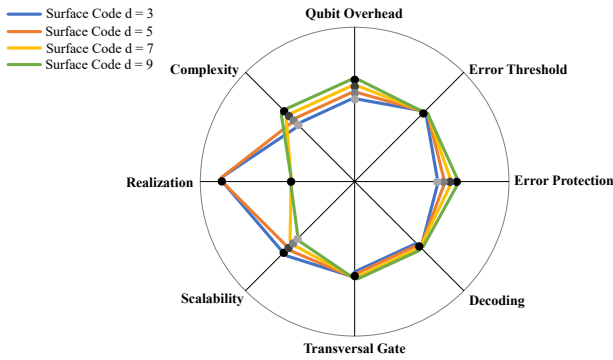


Figure 12: **Radar chart representing comparative analysis of four surface codes across eight parameters.** The parameter axes radiating from the center are as follows: Qubit Overhead ( $d^2$ ) = {9, 25, 49, 81}; Error Threshold =  $\{10^{-2}\}$ ; Error Protection = {all Pauli errors with increasing degree}; Decoding = {10+}; Transversal Gates = {lattice surgery}; Scalability = {'yes' with increasing degree of challenges}; and Realization = {no, yes}.

quired distances to attain specific logical error rates for certain physical error rates. In practical terms, only the 3 and 5 distance surface codes have been implemented to date [9, 63, 42], with higher distances yet to be achieved. While the complexity of surface codes is generally considered high, it increases with distance. The graphs presented were generated through experiments conducted using STIM [31] simulations. Figure 12 presents a radar chart comparing four different surface codes against benchmarking parameters.

It is crucial to recognize that benchmarking is not only vital for evaluating different types of codes but also for assessing variations within existing codes. The process of selecting a code is dynamic and situational, with no fixed rules. Hence, paying attention to minor differences in codes is as important as considering major codes. In terms of code selection, although a universal solution doesn't exist, we can establish a general hierarchy for benchmarking parameters based on typical priorities: The combined aspects of error protection and threshold typically receive the highest priority. This is followed by qubit overhead and complexity. Next in line are scalability and practical realization. Lastly, transversal gates and the number of decoding algorithms are considered. This ordering works because it aligns with the fundamental requirements of quantum computing, where error management is paramount, followed by resource efficiency (qubit usage and

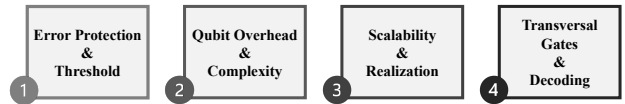


Figure 13: **Strategic prioritization in QECC selection.** This figure emphasizes the critical role of error management and resource efficiency at the top, followed by scalability and practical application, with specialized aspects like transversal gates and decoding algorithms ranked accordingly. This order aids in informed decision-making in code selection.

complexity) and practical feasibility (scalability and realization). Transversal gates and decoding algorithms, while important, are often tailored to specific use cases and thus are considered after these broader concerns. Figure 13 illustrates this prioritization of benchmarking parameters in code selection.

## 5 Future Work and Challenges

The field of quantum error correction is dynamic, continuously yielding diverse types of codes. This paper's contribution — a set of parameters for benchmarking all QECCs — highlights an essential future direction: the evaluation of emerging codes. Understanding a code's practicality and its position relative to existing solutions is crucial. Quantum error correction hinges on achieving a delicate balance; a comprehensive understanding of all parameters is vital for the appropriate application of each code.

Furthermore, the ongoing development in quantum error correction extends to existing codes and their variations. Over time, the realization of current QECCs across a broader spectrum of qubit technologies could alter their standings in the benchmark. While the parameters for evaluation remain constant, their relevance and implications may shift, underscoring the importance of continual updates and assessments in this rapidly evolving field.

## 6 Conclusion

This paper showcases the first universal benchmarking methodology for Quantum Error Correction Codes (QECCs), addressing a significant gap in quantum computing research. By meticulously evaluating eight QECCs against eight carefully

selected parameters, this study not only establishes the importance of these parameters but also provides a nuanced understanding of how each QECC fares in various scenarios. The utilization of a radar chart for comparison vividly illustrates that every QECC involves distinct trade-offs, emphasizing that the selection of a QECC is a complex art of balancing diverse factors. This paper underlines the ongoing necessity of benchmarking as new and variations of QECCs are discovered, reflecting the dynamic nature of quantum computing where QECC selection is highly situational and no single solution prevails. This work is a step forward in ensuring that QECC choices are informed, balanced, and adaptable to evolving quantum computing needs.

## Acknowledgements

The work is supported in parts by the National Science Foundation (NSF) (CNS-1722557, CCF-1718474, OIA-2040667, DGE-1723687, and DGE-1821766).

## References

- [1] Exponential suppression of bit or phase errors with cyclic error correction. *Nature*, 595 (7867):383–387, 2021.
- [2] MH Aboeib, Y Wang, J Randall, SJH Loeenen, CE Bradley, M Markham, DJ Twitchen, BM Terhal, and TH Taminiau. Fault-tolerant operation of a logical qubit in a diamond quantum processor. *Nature*, 606 (7916):884–889, 2022.
- [3] Dorit Aharonov and Michael Ben-Or. Fault-tolerant quantum computation with constant error. In *Proceedings of the twenty-ninth annual ACM symposium on Theory of computing*, pages 176–188, 1997.
- [4] Akshay Ajagekar and Fengqi You. Quantum computing for energy systems optimization: Challenges and opportunities. *Energy*, 179: 76–89, 2019.
- [5] Panos Aliferis and Andrew W Cross. Subsystem fault tolerance with the bacon-shor code. *Physical review letters*, 98(22):220502, 2007.
- [6] Dave Bacon. Operator quantum error-correcting subsystems for self-correcting quantum memories. *Physical Review A*, 73 (1):012340, 2006.
- [7] Lucas Berent, Lukas Burgholzer, Peter-Jan HS Derks, Jens Eisert, and Robert Wille. Decoding quantum color codes with maxsat. *arXiv preprint arXiv:2303.14237*, 2023.
- [8] Debasmita Bhoumik, Ritajit Majumdar, Dhiraj Madan, Dhinakaran Vinayagamurthy, Shesha Raghunathan, and Susmita Sur-Kolay. Efficient machine-learning-based decoder for heavy hexagonal qecc. *arXiv preprint arXiv:2210.09730*, 2022.
- [9] Dolev Bluvstein, Harry Levine, Giulia Semeghini, Tout T Wang, Sepehr Ebadi, Marcin Kalinowski, Alexander Keesling, Nishad Maskara, Hannes Pichler, Markus Greiner, et al. A quantum processor based on coherent transport of entangled atom arrays. *Nature*, 604(7906):451–456, 2022.
- [10] Héctor Bombín. An introduction to topological quantum codes. *arXiv preprint arXiv:1311.0277*, 2013.
- [11] Hector Bombin and Miguel Angel Martin-Delgado. Topological quantum distillation. *Physical review letters*, 97(18):180501, 2006.
- [12] Sergey Bravyi, Martin Suchara, and Alexander Vargo. Efficient algorithms for maximum likelihood decoding in the surface code. *Physical Review A*, 90(3):032326, 2014.
- [13] A Robert Calderbank and Peter W Shor. Good quantum error-correcting codes exist. *Physical Review A*, 54(2):1098, 1996.
- [14] Christopher Chamberland, Aleksander Kubica, Theodore J Yoder, and Guanyu Zhu. Triangular color codes on trivalent graphs with flag qubits. *New Journal of Physics*, 22(2):023019, 2020.
- [15] Christopher Chamberland, Guanyu Zhu, Theodore J Yoder, Jared B Hertzberg, and Andrew W Cross. Topological and subsystem codes on low-degree graphs with flag qubits. *Physical Review X*, 10(1):011022, 2020.
- [16] Avimita Chatterjee, Subrata Das, and Swaroop Ghosh. Q-pandora unboxed: Characterizing noise resilience of quantum error correction codes. 2023.
- [17] Avimita Chatterjee, Koustubh Phalak, and Swaroop Ghosh. Quantum error cor-

- rection for dummies. *arXiv preprint arXiv:2304.08678*, 2023.
- [18] John Chiaverini, Dietrich Leibfried, Tobias Schaetz, Murray D Barrett, RB Blakestad, Joseph Britton, Wayne M Itano, John D Jost, Emanuel Knill, Christopher Langer, et al. Realization of quantum error correction. *Nature*, 432(7017):602–605, 2004.
- [19] Aashish A Clerk, Michel H Devoret, Steven M Girvin, Florian Marquardt, and Robert J Schoelkopf. Introduction to quantum noise, measurement, and amplification. *Reviews of Modern Physics*, 82(2):1155, 2010.
- [20] Ian Convy, Haoran Liao, Song Zhang, Sahil Patel, William P Livingston, Ho Nam Nguyen, Irfan Siddiqi, and K Birgitta Whaley. Machine learning for continuous quantum error correction on superconducting qubits. *New Journal of Physics*, 24(6):063019, 2022.
- [21] Nicolas Delfosse and Naomi H Nickerson. Almost-linear time decoding algorithm for topological codes. *Quantum*, 5:595, 2021.
- [22] Eric Dennis, Alexei Kitaev, Andrew Landahl, and John Preskill. Topological quantum memory. *Journal of Mathematical Physics*, 43(9):4452–4505, 2002.
- [23] Simon J Devitt, William J Munro, and Kae Nemoto. Quantum error correction for beginners. *Reports on Progress in Physics*, 76(7):076001, 2013.
- [24] DGBJ Dieks. Communication by epr devices. *Physics Letters A*, 92(6):271–272, 1982.
- [25] Guillaume Duclos-Cianci and David Poulin. Fast decoders for topological quantum codes. *Physical review letters*, 104(5):050504, 2010.
- [26] Laird Egan, Dripto M Debroy, Crystal Noel, Andrew Risinger, Daiwei Zhu, Debopriyo Biswas, Michael Newman, Muyuan Li, Kenneth R Brown, Marko Cetina, et al. Fault-tolerant operation of a quantum error-correction code. *arXiv preprint arXiv:2009.11482*, 2020.
- [27] Austin G Fowler. Minimum weight perfect matching of fault-tolerant topological quantum error correction in average  $o(1)$  parallel time. *arXiv preprint arXiv:1307.1740*, 2013.
- [28] Austin G Fowler, Matteo Mariantoni, John M Martinis, and Andrew N Cleland. Surface codes: Towards practical large-scale quantum computation. *Physical Review A*, 86(3):032324, 2012.
- [29] Michael H Freedman and David A Meyer. Projective plane and planar quantum codes. *Foundations of Computational Mathematics*, 1:325–332, 2001.
- [30] Phillip Gachnang, Joachim Ehrental, Thomas Hanne, and Rolf Dornberger. Quantum computing in supply chain management state of the art and research directions. *Asian Journal of Logistics Management*, 1(1):57–73, 2022.
- [31] Craig Gidney. Stim: a fast stabilizer circuit simulator. *Quantum*, 5:497, 2021.
- [32] Daniel Gottesman. *Stabilizer codes and quantum error correction*. California Institute of Technology, 1997.
- [33] Richard W Hamming. Error detecting and error correcting codes. *The Bell system technical journal*, 29(2):147–160, 1950.
- [34] James William Harrington. *Analysis of quantum error-correcting codes: symplectic lattice codes and toric codes*. California Institute of Technology, 2004.
- [35] Matthew B Hastings, Jeongwan Haah, and Ryan O’Donnell. Fiber bundle codes: breaking the  $n^{1/2}$  polylog( $n$ ) barrier for quantum ldpc codes. In *Proceedings of the 53rd Annual ACM SIGACT Symposium on Theory of Computing*, pages 1276–1288, 2021.
- [36] Bettina Heim, Krysta M Svore, and Matthew B Hastings. Optimal circuit-level decoding for surface codes. *arXiv preprint arXiv:1609.06373*, 2016.
- [37] Oscar Higgott, Thomas C Bohdanowicz, Aleksander Kubica, Steven T Flammia, and Earl T Campbell. Improved decoding of circuit noise and fragile boundaries of tailored surface codes. *Physical Review X*, 13(3):031007, 2023.
- [38] Dominic Horsman, Austin G Fowler, Simon Devitt, and Rodney Van Meter. Surface code quantum computing by lattice surgery. *New Journal of Physics*, 14(12):123011, 2012.
- [39] Adrian Hutter, James R Wootton, and Daniel Loss. Efficient markov chain monte carlo algorithm for the surface code. *Physical Review A*, 89(2):022326, 2014.
- [40] A Yu Kitaev. Quantum computations: algo-

- rithms and error correction. *Russian Mathematical Surveys*, 52(6):1191, 1997.
- [41] A Yu Kitaev. Fault-tolerant quantum computation by anyons. *Annals of physics*, 303(1):2–30, 2003.
- [42] Sebastian Krinner, Nathan Lacroix, Ants Remm, Agustin Di Paolo, Elie Genois, Catherine Leroux, Christoph Hellings, Stefania Lazar, Francois Swiadek, Johannes Herrmann, et al. Realizing repeated quantum error correction in a distance-three surface code. *Nature*, 605(7911):669–674, 2022.
- [43] Aleksander Kubica, Beni Yoshida, and Fernando Pastawski. Unfolding the color code. *New Journal of Physics*, 17(8):083026, 2015.
- [44] Aleksander Marek Kubica. *The ABCs of the color code: A study of topological quantum codes as toy models for fault-tolerant quantum computation and quantum phases of matter*. PhD thesis, California Institute of Technology, 2018.
- [45] Hoi-Kwong Lo, Tim Spiller, and Sandu Popescu. *Introduction to quantum computation and information*. World Scientific, 1998.
- [46] Yi-Han Luo, Ming-Cheng Chen, Manuel Erhard, Han-Sen Zhong, Dian Wu, Hao-Yang Tang, Qi Zhao, Xi-Lin Wang, Keisuke Fujii, Li Li, et al. Quantum teleportation of physical qubits into logical code spaces. *Proceedings of the National Academy of Sciences*, 118(36):e2026250118, 2021.
- [47] G Mouloudakis and P Lambropoulos. Entanglement instability in the interaction of two qubits with a common non-markovian environment. *Quantum Information Processing*, 20:1–15, 2021.
- [48] Jonathan E Moussa. Transversal clifford gates on folded surface codes. *Physical Review A*, 94(4):042316, 2016.
- [49] Mikio Nakahara, Yidun Wan, and Yoshitaka Sasaki. *Diversities in Quantum Computation and Quantum Information*, volume 5. World Scientific, 2012.
- [50] Nhung H Nguyen, Muyuan Li, Alaina M Green, C Huerta Alderete, Yingyue Zhu, Daiwei Zhu, Kenneth R Brown, and Norbert M Linke. Demonstration of shor encoding on a trapped-ion quantum computer. *Physical Review Applied*, 16(2):024057, 2021.
- [51] Michael A Nielsen and Isaac L Chuang. Quantum computation and quantum information. *Phys. Today*, 54(2):60, 2001.
- [52] Daniel Nigg, Markus Mueller, Esteban A Martinez, Philipp Schindler, Markus Henrich, Thomas Monz, Miguel A Martin-Delgado, and Rainer Blatt. Quantum computations on a topologically encoded qubit. *Science*, 345(6194):302–305, 2014.
- [53] Josias Old and Manuel Risper. Generalized belief propagation algorithms for decoding of surface codes. *Quantum*, 7:1037, 2023.
- [54] Román Orús, Samuel Muel, and Enrique Lizaso. Quantum computing for finance: Overview and prospects. *Reviews in Physics*, 4:100028, 2019.
- [55] Asher Peres. Reversible logic and quantum computers. *Physical review A*, 32(6):3266, 1985.
- [56] John Preskill. Reliable quantum computers. *Proceedings of the Royal Society of London. Series A: Mathematical, Physical and Engineering Sciences*, 454(1969):385–410, 1998.
- [57] Matthew D Reed, Leonardo DiCarlo, Simon E Nigg, Luyan Sun, Luigi Frunzio, Steven M Girvin, and Robert J Schoelkopf. Realization of three-qubit quantum error correction with superconducting circuits. *Nature*, 482(7385):382–385, 2012.
- [58] Markus Reiher, Nathan Wiebe, Krysta M Svore, Dave Wecker, and Matthias Troyer. Elucidating reaction mechanisms on quantum computers. *Proceedings of the national academy of sciences*, 114(29):7555–7560, 2017.
- [59] Joschka Roffe. Quantum error correction: an introductory guide. *Contemporary Physics*, 60(3):226–245, 2019.
- [60] Jonathan F San Miguel, Dominic J Williamson, and Benjamin J Brown. A cellular automaton decoder for a noise-bias tailored color code. *Quantum*, 7:940, 2023.
- [61] Albert T Schmitz. Thermal stability of dynamical phase transitions in higher dimensional stabilizer codes. *arXiv preprint arXiv:2002.11733*, 2020.
- [62] Maria Schuld, Ilya Sinayskiy, and Francesco Petruccione. An introduction to quantum machine learning. *Contemporary Physics*, 56(2):172–185, 2015.
- [63] Giulia Semeghini, Harry Levine, Alexander Keesling, Sephehr Ebadi, Tout T Wang,

- Dolev Bluvstein, Ruben Verresen, Hannes Pichler, Marcin Kalinowski, Rhine Samajdar, et al. Probing topological spin liquids on a programmable quantum simulator. *Science*, 374(6572):1242–1247, 2021.
- [64] Peter W Shor. Scheme for reducing decoherence in quantum computer memory. *Physical review A*, 52(4):R2493, 1995.
- [65] Andrew Steane. Multiple-particle interference and quantum error correction. *Proceedings of the Royal Society of London. Series A: Mathematical, Physical and Engineering Sciences*, 452(1954):2551–2577, 1996.
- [66] Andrew M Steane. Error correcting codes in quantum theory. *Physical Review Letters*, 77(5):793, 1996.
- [67] Ashley M Stephens. Efficient fault-tolerant decoding of topological color codes. *arXiv preprint arXiv:1402.3037*, 2014.
- [68] Martin Suchara, Arvin Faruque, Ching-Yi Lai, Gerardo Paz, Frederic Chong, and John D Kubiatowicz. Estimating the resources for quantum computation with the qure toolbox. *EECS Department, University of California, Berkeley (accessed 2 October 2018) <http://www2.eecs.berkeley.edu/Pubs/TechRpts/2013/EECS-2013-119.html>*, 2013.
- [69] Neereja Sundaresan, Theodore J Yoder, Youngseok Kim, Muyuan Li, Edward H Chen, Grace Harper, Ted Thorbeck, Andrew W Cross, Antonio D Córcoles, and Maika Takita. Matching and maximum likelihood decoding of a multi-round subsystem quantum error correction experiment. *arXiv preprint arXiv:2203.07205*, 2022.
- [70] Neereja Sundaresan, Theodore J Yoder, Youngseok Kim, Muyuan Li, Edward H Chen, Grace Harper, Ted Thorbeck, Andrew W Cross, Antonio D Córcoles, and Maika Takita. Demonstrating multi-round subsystem quantum error correction using matching and maximum likelihood decoders. *Nature Communications*, 14(1):2852, 2023.
- [71] Xinyu Tan, Fang Zhang, Rui Chao, Yaoyun Shi, and Jianxin Chen. Scalable surface-code decoders with parallelization in time. *PRX Quantum*, 4(4):040344, 2023.
- [72] Barbara M Terhal. Quantum error correction for quantum memories. *Reviews of Modern Physics*, 87(2):307, 2015.
- [73] Yu Tomita and Krysta M Svore. Low-distance surface codes under realistic quantum noise. *Physical Review A*, 90(6):062320, 2014.
- [74] Andrei L Toom. Nonergodic multidimensional system of automata. *Problemy Peredachi Informatsii*, 10(3):70–79, 1974.
- [75] Giacomo Torlai and Roger G Melko. Neural decoder for topological codes. *Physical review letters*, 119(3):030501, 2017.
- [76] John Von Neumann. *Mathematical foundations of quantum mechanics: New edition*, volume 53. Princeton university press, 2018.
- [77] Gerald Waldherr, Ya Wang, S Zaiser, M Jamali, T Schulte-Herbrüggen, H Abe, T Ohshima, J Isoya, JF Du, P Neumann, et al. Quantum error correction in a solid-state hybrid spin register. *Nature*, 506(7487):204–207, 2014.
- [78] William K Wootters and Wojciech H Zurek. A single quantum cannot be cloned. *Nature*, 299(5886):802–803, 1982.
- [79] William K Wootters and Wojciech H Zurek. The no-cloning theorem. *Physics Today*, 62(2):76–77, 2009.
- [80] Shibo Xu, Zheng-Zhi Sun, Ke Wang, Liang Xiang, Zehang Bao, Zitian Zhu, Fanhao Shen, Zixuan Song, Pengfei Zhang, Wenhui Ren, et al. Digital simulation of projective non-abelian anyons with 68 superconducting qubits. *Chinese Physics Letters*, 2023.
- [81] Bei Zeng, Andrew Cross, and Isaac L Chuang. Transversality versus universality for additive quantum codes. *IEEE Transactions on Information Theory*, 57(9):6272–6284, 2011.
- [82] Jingfu Zhang, Dorian Gangloff, Osama Moussa, and Raymond Laflamme. Experimental quantum error correction with high fidelity. *Physical Review A*, 84(3):034303, 2011.
- [83] Xinlan Zhou, Debbie W Leung, and Isaac L Chuang. Methodology for quantum logic gate construction. *Physical Review A*, 62(5):052316, 2000.